

HD-TESS: An Asteroseismic Catalog of Bright Red Giants within TESS Continuous Viewing Zones

MARC HON ^{1,*}, JAMES S. KUSZLEWICZ ^{2,3,4}, DANIEL HUBER ¹, DENNIS STELLO ^{5,3,6,7} AND CLAUDIA REYES⁵

¹*Institute for Astronomy, University of Hawai‘i, 2680 Woodlawn Drive, Honolulu, HI 96822, USA*

²*Center for Astronomy (Landessternwarte), Heidelberg University, Königstuhl 12, 69118 Heidelberg, Germany*

³*Stellar Astrophysics Centre, Department of Physics and Astronomy, Aarhus University, Ny Munkegade 120, DK-8000 Aarhus C, Denmark*

⁴*Max-Planck-Institut für Sonnensystemforschung, Justus-von-Liebig-Weg 3, 37077 Göttingen, Germany*

⁵*School of Physics, The University of New South Wales, Sydney NSW 2052, Australia*

⁶*Sydney Institute for Astronomy (SfA), School of Physics, University of Sydney, NSW 2006, Australia*

⁷*ARC Centre of Excellence for Astrophysics in Three Dimensions (ASTRO-3D), Australia*

ABSTRACT

We present HD-TESS, a catalog of 1,709 bright ($V \sim 3 - 10$) red giants from the Henry Draper (HD) Catalog with asteroseismic measurements based on photometry from NASA’s Transiting Exoplanet Survey Satellite (TESS). Using light curves spanning at least six months across a single TESS observing cycle, we provide measurements of global asteroseismic parameters (ν_{\max} and $\Delta\nu$) and evolutionary state for each star in the catalog. We adopt literature values of atmospheric stellar parameters to estimate the masses and radii of the giants in our catalog using asteroseismic scaling relations, and observe that HD-TESS giants on average have larger masses compared to *Kepler* red giants. Additionally, we present the discovery of oscillations in 99 red giants in astrometric binary systems, including those with subdwarf or white dwarf companions. Finally, we benchmark radii from asteroseismic scaling relations against those measured using long-baseline interferometry for 18 red giants and find that correction factors to the scaling relations improve the agreement between asteroseismic and interferometric radii to approximately 3%.

Keywords: asteroseismology — stars: oscillations — methods: data analysis

1. INTRODUCTION

Bright stars are amongst some of the most well-studied celestial objects. They are prime targets for a myriad of studies, including high-resolution spectroscopic surveys of the solar neighbourhood (e.g., Luck & Heiter 2007; Hekker & Meléndez 2007; Soubiran et al. 2010; Feuillet et al. 2018) as well as planet searches using the Doppler velocity method (e.g., Pepe et al. 2011; Addison et al. 2019). Furthermore, fundamental measurements such as angular diameters (e.g., Baines et al. 2010; von Braun & Boyajian 2017), and dynamical measurements of visual binaries (e.g., McAlister 1977; Retterer & King 1982; Mason et al. 2001) are limited to only bright stars. Some of these stars additionally serve

as benchmarks for studying stellar populations in the Galaxy (Jofré et al. 2018), and therefore a precise characterization of their properties is essential.

Asteroseismology, the study of stellar oscillations, can provide precise measurements of the masses and radii of Sun-like stars (Christensen-Dalsgaard 1984; Bedding 2014; García & Stello 2015; Chaplin et al. 2014; Hekker & Christensen-Dalsgaard 2017). Over the past decade, the availability of precise, continuous photometry from space missions CoRoT (Baglin et al. 2009), *Kepler* (Borucki et al. 2010) and *K2* (Howell et al. 2014) has enabled the seismic characterization of the fundamental properties of thousands of red giants across distant stellar populations within the Milky Way (Miglio et al. 2009; Pinsonneault et al. 2018; Yu et al. 2018), which has been pivotal in studies of Galactic archeology (e.g., Silva Aguirre et al. 2018; Zinn et al. 2020; Miglio et al. 2021). However, the asteroseismology of bright ($V \lesssim 7$) stars has previously been limited to only several dozens of tar-

Corresponding author: Marc Hon
mtyhon@hawaii.edu

* NASA Hubble Fellow

gets that can be measured from ground-based radial velocity surveys (e.g., Kjeldsen et al. 1995; Frandsen et al. 2002; Malla et al. 2020), or a small subset of *Kepler*/*K2* stars for which smear and halo photometry can be applied (Pope et al. 2016; White et al. 2017; Pope et al. 2019). It is only through recent space-borne photometric surveys specifically targeting bright stars such as the Bright Target Explorer (Weiss et al. 2014, BRITE) and NASA’s Transiting Exoplanet Survey Satellite (Ricker et al. 2015, TESS) that the asteroseismology of a large ensemble of bright stars is now possible.

In this paper, we aim to characterize the fundamental parameters of bright red giants observed by TESS. The prime targets for this analysis are stars near or within the TESS Continuous Viewing Zones (CVZs), which are parts of the sky with maximal overlap between the $24^\circ \times 96^\circ$ TESS observing fields (sectors) within Cycles 1-3 of the mission. The long photometric time series resulting from this overlap lead to a greater frequency resolution in the Fourier domain, which in turn improves the precision of asteroseismic measurements. As a result, we aim to produce a catalog of seismically-determined masses and radii for bright red giants that will be useful for informing other studies involving giant stars. This catalog also seeks to complement previous asteroseismic studies of red giants with TESS — specifically the work by Silva Aguirre et al. (2020) that measured the oscillation properties of 25 bright red giants, the Galactic archeology study by Mackereth et al. (2021) that seismically analyzed $\sim 5,500$ red giants in the southern CVZ, and the near all-sky detection and seismic characterization of $\sim 158,000$ giants by Hon et al. (2021). In contrast to these studies, we will focus on the bright stars in both CVZs by basing our selection on red giants from the Henry Draper (HD) catalog (Cannon & Pickering 1993; Nesterov et al. 1995). The cross-match between our selection from the HD catalog with TESS observations thus yields the HD-TESS catalog whose construction we detail in the following.

2. DATA

There are two sources of light curves in this study. The first is the TESS Science Processing Operations Center pipeline (Twicken et al. 2016; Jenkins 2020, SPOC) obtained from the Mikulski Archive for Space Telescopes (MAST) at the Space Telescope Science Institute, accessed via [doi:10.17909/t9-nmc8-f686](https://doi.org/10.17909/t9-nmc8-f686). The second is the MIT Quick-Look Pipeline (Huang et al. 2020a,b, QLP), accessed via [doi:10.17909/t9-r086-e880](https://doi.org/10.17909/t9-r086-e880). Generally, we find that SPOC light curves better preserve flux variability corresponding to giant oscillations for bright and saturated targets with $T_{\text{mag}} \lesssim 7$ compared to those from

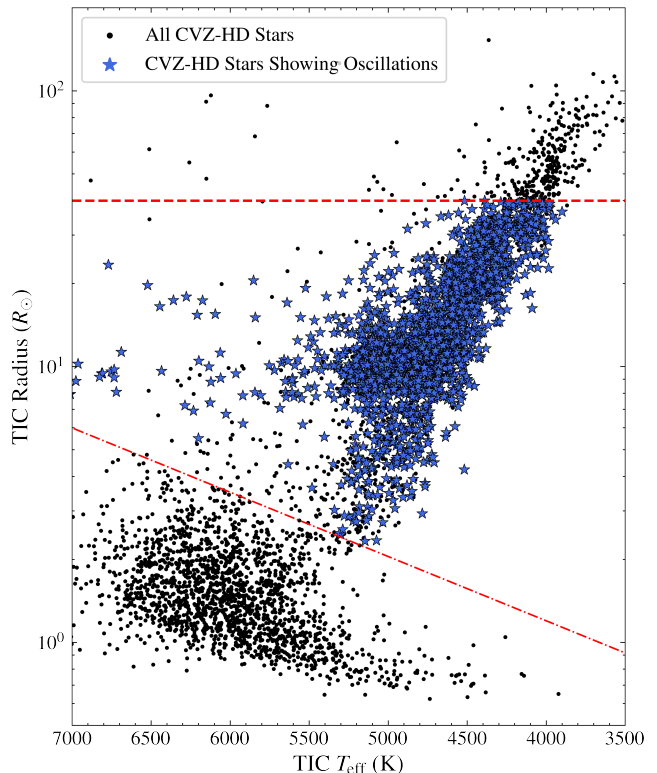


Figure 1. Stellar radius versus effective temperature for stars with spectral type G-K from the Henry Draper catalog that have been observed for at least six sectors in Cycles 1+2 from TESS and therefore lie near or within the TESS Continuous Viewing Zones (CVZs). The temperatures and radii in this plot are from the TESS Input Catalog (Stassun et al. 2019, TIC). Stars in our sample are those that lie between the two lines in this diagram whereby the upper line corresponds to a $40R_\odot$ radius cut-off, while the lower line corresponds to a fiducial boundary separating early subgiants from the base of the red giant branch (see text). The blue points correspond to stars that show a power excess corresponding to red giant oscillations in their power spectrum.

the MIT Quick-Look Pipeline (Huang et al. 2020a,b, QLP). Many of the fainter HD stars in our sample, however, were not targeted by the SPOC pipeline but have light curves generated from the QLP. Because the data from QLP’s simple aperture photometry is generally adequate for observing giant oscillations at fainter magnitudes (Hon et al. 2021), our approach here is to prioritize SPOC light curves whenever possible, otherwise we default to QLP photometry.

Our analysis includes observations up to Sector 39 for stars with SPOC light curves, such that stars near the southern ecliptic poles will have up to two years of data as of the end of the year 2021. For stars having only QLP photometry, we use data across Cycles 1 and 2, meaning the maximum length of the time series for such stars in this work will be one year. Although QLP light curves

across Cycle 3 are available (Kunimoto et al. 2021), the data have a reduced sampling cadence of 10 minutes as opposed to the 30-minute cadence across the first two TESS Cycles. To simplify the treatment of data in this study, we incorporate a consistent observing cadence for each star’s light curve and therefore delegate the task of matching difference observing cadences as part of future work.

3. TARGET SELECTION

First, we identify 5,711 stars with spectral types G and K from the HD catalog that have been observed for at least six sectors in TESS Cycles 1 and 2. Next, we impose a selection based on a star’s effective temperature and radius from the TESS Input Catalog version 8.2 (Stassun et al. 2019, TIC), as follows:

- $R < 40 R_{\odot}$ as an upper boundary to filter out long-period variables.
- $R \geq 10^p R_{\odot}$, with $p = (\frac{T_{\text{eff}}(\text{K})}{7000} - \frac{3}{7}) \log(\frac{300}{7}) + \log(0.7)$. This is the boundary used by Hon et al. (2019) to discriminate early subgiant stars from those beginning to ascend the red giant branch.

This selection is depicted in Figure 1. Under this selection, we reduce the initial sample of stars to 3,142, from which 2,611 show red giant oscillations. Note that 2,042 of the 2,611 stars are already known to show oscillations based on previous work by Hon et al. (2021). This implies that 569 red giants in this sample are new inclusions that were not previously detected from one month of TESS data.

3.1. Asteroseismic Measurements

We extract initial estimates for the frequency at maximum oscillation power (ν_{max}), and the large frequency separation ($\Delta\nu$) for the sample of 2,611 giants using the SYD asteroseismic data pipeline (Huber et al. 2009). With improvements to the SYD pipeline as specified in Huber et al. (2011) and Yu et al. (2018), the pipeline has previously been applied for the asteroseismology of shorter time series including those from *K2* (Zinn et al. 2020, 2022) and even from TESS itself (Stello et al. 2021). Beginning with the SYD pipeline’s ν_{max} estimates, we further refine the estimates by performing a Bayesian fit using a model comprising a Gaussian envelope with three background components to the star’s power spectrum as described by Themeßl et al. (2020). The resulting ν_{max} from this final fit is our reported estimate.

The raw output from the SYD pipeline reports a $\Delta\nu$ measured automatically from the autocorrelation function of the oscillation power spectrum for each input

star. However, complicating features in the frequency domain such as lower signal-to-noise ratios, additional mode structure from dipole mixed modes (e.g., Bedding et al. 2011), or the overlap of other periodic signals unrelated to oscillations (e.g., Colman et al. 2017) may result in inaccurate measurements of $\Delta\nu$. To avoid such occurrences, we first vet the SYD pipeline outputs using the neural network classifier introduced by Reyes et al. (2022). Briefly, the classifier takes as input extracted features across a variety of commonly used visual diagrams in asteroseismology — such as the autocorrelation plot and the échelle diagram of the oscillation modes — and subsequently outputs a probability indicating whether the $\Delta\nu$ measurement used to construct such diagrams corresponds to a valid measurement. To further ensure the robustness of the $\Delta\nu$ measurements, we additionally inspect the oscillation spectrum of each star using diagnostic plots such as shown in Figure 2. We perform this inspection in addition to the automatic vetting by the neural network because it allows us to recover a fraction of initially rejected stars that have $\Delta\nu$ erroneously estimated by the seismic pipeline (and thus rightfully rejected by the automatic vetting). To recover $\Delta\nu$ for such stars, we manually tune $\Delta\nu$ such that: (1) vertical ridges are formed in the échelle diagram; (2) peaks are observed at 1 and 2 $\Delta\nu$ in the autocorrelation of the oscillation spectrum, as indicated in Figure 2. The uncertainty in $\Delta\nu$ is taken as the shift required to disrupt the vertical alignment of the ridges in the échelle diagram and is approximately at the 2-3% level. We additionally inspect other stars that pass the automatic vetting to ensure that the same visual criteria are met.

The result of the vetting is shown in Figure 3. From 2,611 oscillating giants, we retain 1,709 for which their $\Delta\nu$ can be identified with a high level of confidence. Most giants filtered out in this vetting stage are those with $R \gtrsim 20R_{\odot}$ (corresponding to $\nu_{\text{max}} \lesssim 10\mu\text{Hz}$) and therefore have long-period oscillations for which frequency separations are typically difficult to measure with one to two years of data. We also observe a sharp cutoff corresponding to an absence of faint stars with small radii, where stars beyond this limit show too low signal-to-noise to have detectable oscillations (Stello et al. 2017; Hon et al. 2021; Stello et al. 2022).

Finally, we categorize the giants in our sample as either those that are hydrogen shell-burning while ascending the red giant branch (RGB) or core helium-burning stars within the red/secondary clump (CHeB) by applying the Hon et al. (2017, 2018) deep learning classifier, which uses the frequency distribution of oscillation modes within a star’s collapsed échelle diagram (e.g.,

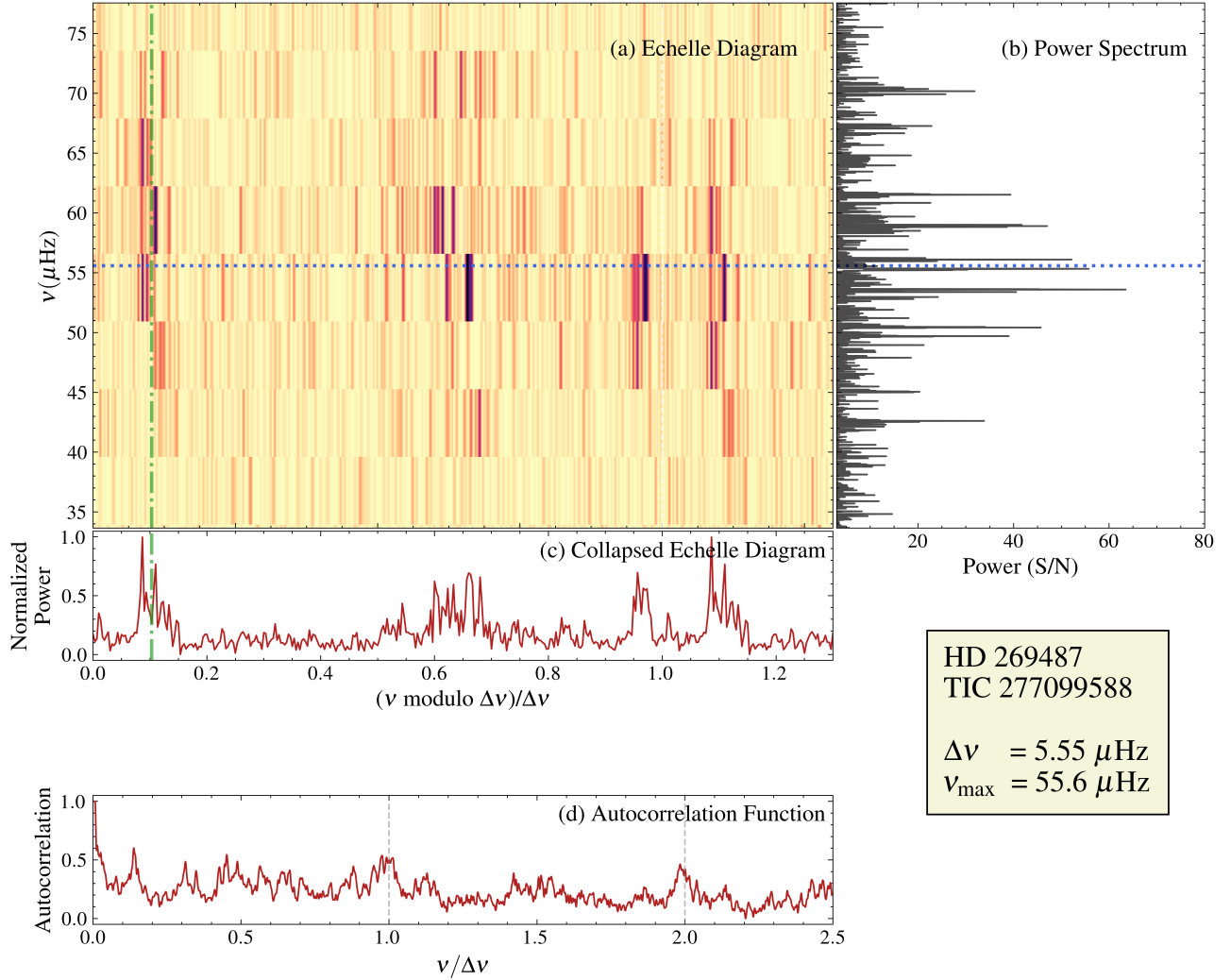


Figure 2. Diagnostic plot for HD 269487 (TIC 277099588) showing (a) an échelle diagram of the (b) oscillation spectrum of the star, (c) the collapsed échelle diagram computed as the summation of power across each row in the échelle diagram, and (d) the autocorrelation function, constructed by convolving the oscillation spectrum in (b) with itself. The échelle diagrams are replicated up to $(\nu \bmod \Delta\nu)/\Delta\nu = 1.25$ to better visualize the repetition of the ridges across radial orders. The blue horizontal line in panels (a) and (b) corresponds to ν_{max} , while the green vertical line in panels (a) and (c) corresponds to the position of the radial mode-ridge in the échelle diagrams, also known as the offset ϵ . The vertical lines in panel (d) correspond to spacings of 1 and 2 $\Delta\nu$, and is where peaks are expected if there is strong regularity in the oscillation spectrum given a candidate $\Delta\nu$ value.

Figure 2c) to determine an evolutionary state. The 1,709 stars with $\Delta\nu$, ν_{max} , and evolutionary state determinations thus forms the HD-TESS catalog and are tabulated in Table 1. The ν_{max} measurements of all 2,611 oscillating giants identified in this study, including those whose $\Delta\nu$ cannot be reliably measured, is tabulated in Appendix A.

4. FUNDAMENTAL STELLAR PARAMETERS

4.1. Seismic Measurements

Figure 4 shows the results of our seismic measurements, where we plot ν_{max} against the quantity $\nu_{\text{max}}^{0.75}/\Delta\nu \sim M^{0.25}T_{\text{eff}}^{-0.375}$, which acts as a temperature (T_{eff})-dependent proxy for stellar mass (M). With TESS observations spanning at least 6 months within the CVZs, we are able to clearly distinguish between RGB and CHeB populations as predicted by Mosser et al. (2019). Other population-level features that are well-resolved from the figure includes the sharpness of the right edge of the CHeB distribution that marks the zero-age CHeB phase (e.g., Kallinger et al. 2010; Li et al. 2021) as well as an overdensity of RGB stars at $\sim 50\mu\text{Hz}$ indicating the luminosity bump in first ascent giants

Table 1. Asteroseismic quantities for 1,709 stars in the HD-TESS catalog. Quantities κ_M and κ_R correspond respectively to mass and radius ‘coefficients’, which are convenient quantities for estimating masses and radii using the asteroseismic scaling relations (Equations 1 and 2). The evolutionary phase of each giant is provided as either hydrogen shell-burning (RGB) or core helium-burning (CHeB). The full version of this table is available in a machine-readable format in the online journal, with a portion shown here for guidance regarding its form and content.

HD number	TIC	T _{mag}	$\Delta\nu$	ν_{\max}	κ_M	κ_R	Phase
		(mag)	(μHz)	(μHz)			
22349	31852879	8.6	3.82 ± 0.04	34.04 ± 0.50	2.10 ± 0.13	13.79 ± 0.35	RGB
23128	238180822	6.6	3.05 ± 0.04	25.24 ± 0.39	2.10 ± 0.15	16.03 ± 0.49	RGB
23381	31960832	7.5	3.59 ± 0.02	30.97 ± 0.50	2.02 ± 0.11	14.19 ± 0.28	CHeB
23399	425997943	7.9	4.18 ± 0.04	34.24 ± 1.39	1.48 ± 0.19	11.58 ± 0.52	CHeB
...
311740	271795748	8.4	7.38 ± 0.02	80.52 ± 0.78	1.99 ± 0.06	8.73 ± 0.10	RGB
370635	370115759	10.9	2.85 ± 0.02	22.95 ± 0.35	2.07 ± 0.11	16.7 ± 0.35	RGB

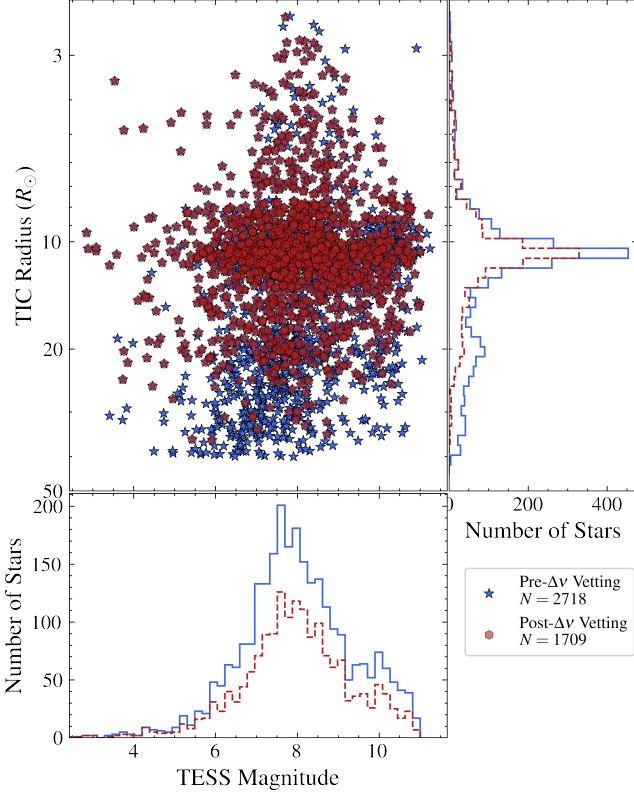


Figure 3. (Left) Radius-magnitude distribution of oscillating giants before (blue) and after (red) vetting of their large frequency separations $\Delta\nu$ as described in Section 3.1. Similar to Figure 1, the radii used in the plot are adopted from the TESS Input Catalog. The plot is aligned such that more luminous giants (with smaller ν_{\max}) are lower, consistent with how the ν_{\max} -magnitude distribution for giants are commonly visualized (e.g., Stello et al. 2017; Zinn et al. 2020; Hon et al. 2021).

(Refsdal & Weigert 1970; Christensen-Dalsgaard 2015; Khan et al. 2018). Additionally, we observe a systematic increase in the stellar mass proxy for both RGB and CHeB TESS populations compared to the giants from *Kepler* (Yu et al. 2018, black points), which we discuss further in Section 4.2.

Estimates of the mass (M) and radius (R) of each giant can be obtained using the following asteroseismic scaling relations:

$$\frac{M}{M_{\odot}} = \left(\frac{\Delta\nu}{f_{\Delta\nu} \Delta\nu_{\odot}} \right)^{-4} \left(\frac{\nu_{\max}}{\nu_{\max,\odot}} \right)^3 \left(\frac{T_{\text{eff}}}{T_{\text{eff},\odot}} \right)^{3/2} = \frac{\kappa_M}{f_{\Delta\nu}^{-4}} \left(\frac{T_{\text{eff}}}{T_{\text{eff},\odot}} \right)^{3/2}, \quad (1)$$

$$\frac{R}{R_{\odot}} = \left(\frac{\Delta\nu}{f_{\Delta\nu} \Delta\nu_{\odot}} \right)^{-2} \left(\frac{\nu_{\max}}{\nu_{\max,\odot}} \right) \left(\frac{T_{\text{eff}}}{T_{\text{eff},\odot}} \right)^{1/2} = \frac{\kappa_R}{f_{\Delta\nu}^{-2}} \left(\frac{T_{\text{eff}}}{T_{\text{eff},\odot}} \right)^{1/2}. \quad (2)$$

These relations are a consequence of the approximate proportionality of $\Delta\nu$ to the square root of stellar mean density (Ulrich 1986) as well as that of ν_{\max} to the star’s acoustic cutoff frequency (Brown et al. 1991; Kjeldsen et al. 1995; Belkacem et al. 2011). The quantity $f_{\Delta\nu}$ is a correction term used to correct for any deviations from the proportionality assumption of the former relation, and has been shown to provide better agreement between independently measured fundamental parameters from eclipsing binaries (Gaulme et al. 2016; Brogaard et al. 2018; Kallinger et al. 2018) and *Gaia* parallaxes (Huber et al. 2017; Hall et al. 2019;

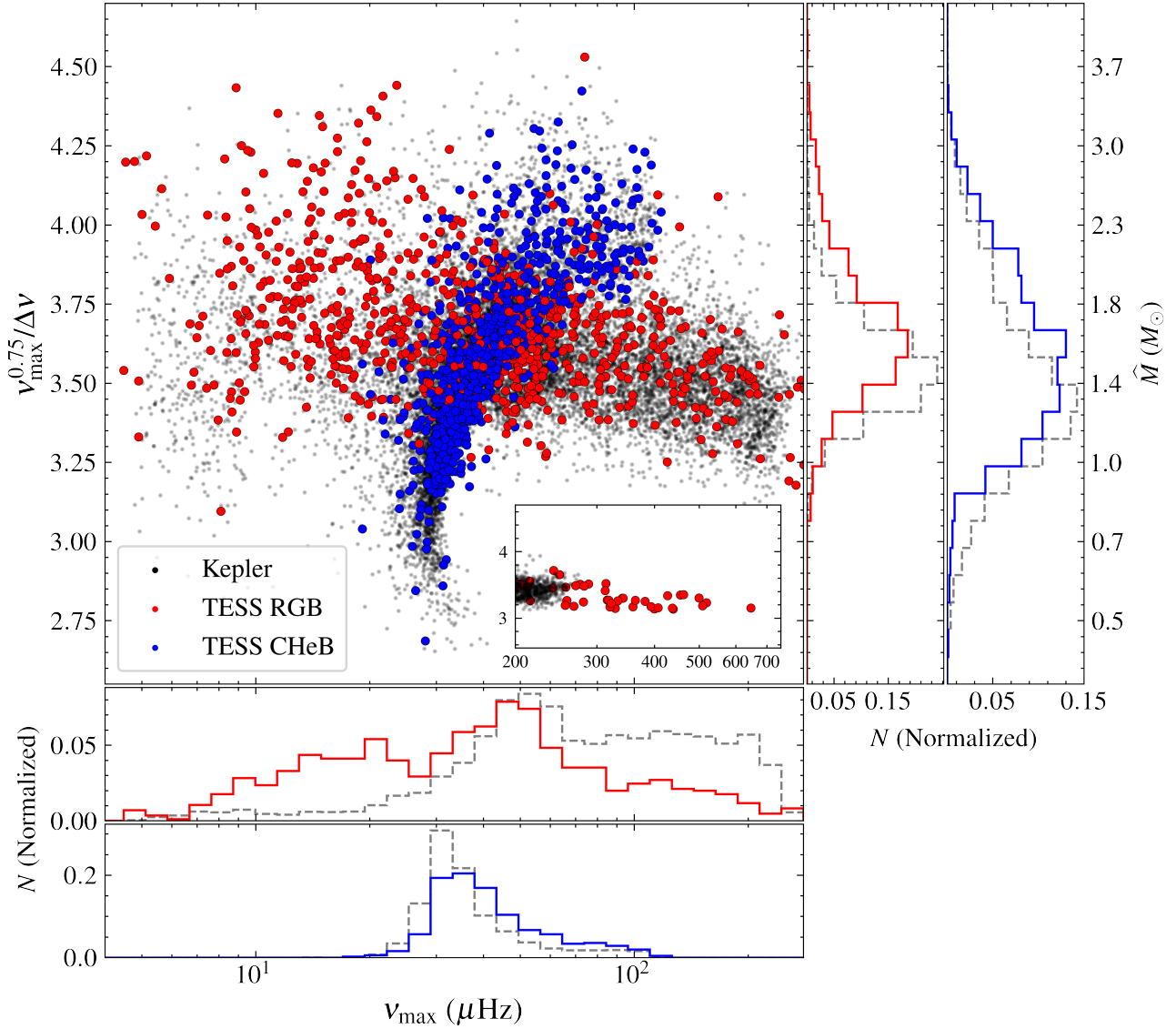


Figure 4. Asteroseismic measurements for the 1,709 stars in the HD-TESS catalog. On the abscissa is frequency at maximum oscillation power (ν_{\max}), while the ordinate $\nu_{\max}^{0.75}/\Delta\nu \sim M^{0.25}T_{\text{eff}}^{-0.375}$ is an asteroseismic proxy for stellar mass. The quantity \hat{M} is the mass proxy computed assuming $T_{\text{eff}} = 5000\text{K}$, shown here to provide an approximation of range of red giant masses reported in this work. In red are hydrogen shell-burning giants ascending the giant branch (RGB), while in blue are core helium-burning giants (CHeB). For comparison, corresponding measurements for *Kepler* red giants (Yu et al. 2018) are shown in gray. The inset shows measurements for low-luminosity TESS giants in our sample.

Zinn et al. 2019). Here, we adopt the solar reference values of $\Delta\nu_{\odot} = 135.1\mu\text{Hz}$, $\nu_{\max,\odot} = 3090\mu\text{Hz}$, and $T_{\text{eff},\odot} = 5777\text{ K}$ (Huber et al. 2011, 2013).

Following Sharma et al. (2016), we condense the scaling relations into a more compact form by defining the coefficients $\kappa_M = (\Delta\nu/\Delta\nu_{\odot})^{-4} \cdot (\nu_{\max}/\nu_{\max,\odot})^3$ for mass and $\kappa_R = (\Delta\nu/\Delta\nu_{\odot})^{-2} \cdot (\nu_{\max}/\nu_{\max,\odot})$ for radius to represent the seismic aspect of both relations. Similar to Zinn et al. (2020), the purpose of reporting such a representation is to provide the user with the choice of using their own atmospheric parameters to estimate

masses and radii. Not only do the scaling relations have an explicit temperature dependence, but the correction term $f_{\Delta\nu}$ is also often computed with reference to stellar models as a function of mass, temperature, metallicity, and evolutionary phase of the star (Sharma et al. 2016; Serenelli et al. 2017; Rodrigues et al. 2017; Li et al. 2022). To obtain cursory estimates of masses and radii in Section 4.2, we adopt the Sharma et al. (2016) correction.

4.2. Estimating Masses and Radii

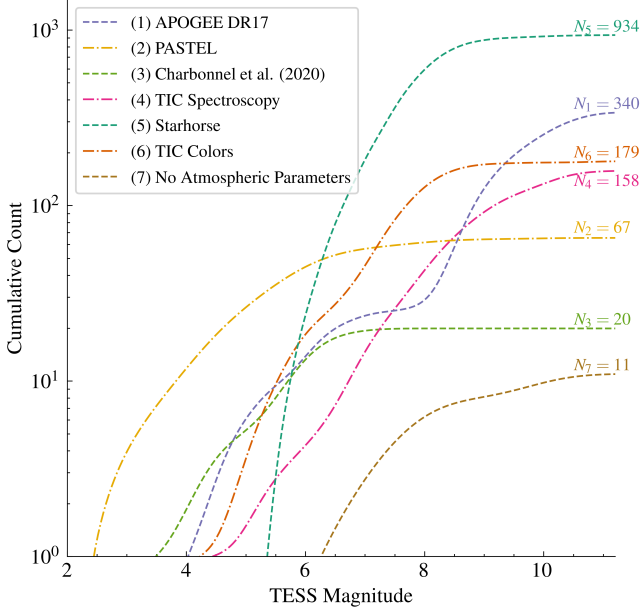


Figure 5. Cumulative histograms of atmospheric parameters sources for HD-TESS giants as a function of TESS magnitude. The number associated with each source in the legend indicates its priority in the selection, while the quantity N enumerates the total number of stars from that particular source. Sources 1-4 provide measurements using spectroscopy, while sources 5 and 6 apply spectrophotometric methods and color-photometry relations, respectively.

A uniform estimation of masses and radii using Equations 1 and 2 for all stars in our sample is not a straightforward task due to the lack of a homogeneous source of atmospheric parameters for such stars. We therefore collect atmospheric parameters from a variety of catalogs as follows, in decreasing priority order:

1. The SDSS/APOGEE-2 Data Release 17 catalog (Abdurro'uf et al. 2022).
2. The PASTEL catalog (Soubiran et al. 2020).
3. Spectroscopic parameters from Charbonnel et al. (2020)
4. Spectroscopic parameters from the TESS Input Catalog, which adopts such measurements across a variety of other spectroscopic catalogs (see Stassun et al. 2018, 2019).
5. Spectrophotometric temperatures and metallicities from the *Starhorse* Bayesian inference tool (Queiroz et al. 2018) based on *Gaia* EDR3 data (Anders et al. 2022).
6. Photometric temperatures from the TESS Input Catalog, which are determined using the color- T_{eff}

relations outlined in Stassun et al. (2019, their Section 2.3.4). Stars in this category have no metallicity information.

A breakdown of the adopted atmospheric parameters from each catalog is shown in Figure 5. Notably, spectroscopic surveys (catalogs 1-4) focus primarily on bright targets with $T_{\text{mag}} \lesssim 6$ or on fainter targets with $T_{\text{mag}} \gtrsim 9$, and therefore lack coverage for intermediate brightness stars within our sample. It is for this reason that we also include atmospheric parameters from spectrophotometric or photometric catalogs for completeness, despite their lack of precision as opposed to spectroscopic measurements (e.g., Figure 18 from Anders et al. 2022). We adopt the reported temperature and metallicity uncertainties from each catalog whenever available. For stars with multiple measurements in the PASTEL catalog, we adopt the standard deviation between the measurements as the uncertainty. Across all atmospheric parameter catalogs, we assign a minimum uncertainty of 0.05 dex for metallicity and 2% for temperature (Tayar et al. 2022).

Given the variety of atmospheric parameter catalogs used, it is difficult to calibrate each to a common temperature or metallicity scale. Although such calibrations can be performed across one large catalog to another (e.g., APOGEE versus *Starhorse*, Anders et al. 2022), spectroscopic catalogs of bright stars such as PASTEL combine measurements across numerous ‘boutique’ surveys, for which systematic differences across each survey are difficult to quantify. We therefore do not make an attempt to calibrate the atmospheric parameters across each catalog to a common scale. Instead, we suggest users to be aware of the origins of the effective temperature and metallicity values used for the mass or radius determination (which we report in Table 2), and to be cautious of systematic offsets between temperatures and metallicity scales between different atmospheric parameter catalogs. For consistency, we recommend the use of κ_M and κ_R from Table 1 along with homogeneously measured atmospheric parameters.

Table 2 tabulates mass and radius for each star using Equations 1 and 2, with $f_{\Delta\nu}$ computed using the Sharma et al. (2016) method, which takes into account the temperature, metallicity, and giant evolutionary state. Here, the quoted uncertainties for masses and radii are estimated from 1σ intervals from Monte Carlo sampling of the scaling relations assuming no correlations between measurements used as inputs. The resulting median uncertainty across our sample is 8.3% for mass and 3.2%

Table 2. Masses and radii for 1,709 red giants in the HD-TESS catalog. The source of atmospheric parameters adopted for each star is indicated by the following: (1)— SDSS/APOGEE-2 DR17 (Abdurro’uf et al. 2022), (2)— PASTEL (Soubiran et al. 2020), (3)— Charbonnel et al. 2020, (4)— TESS Input Catalog (Stassun et al. 2019, TIC) spectroscopy, (5)— *Starhorse Gaia* EDR3 (Queiroz et al. 2018; Anders et al. 2022), (6)— TIC photometric colors, (7)— No atmospheric parameters. The full version of this table is available in a machine-readable format in the online journal, with a portion shown here for guidance regarding its form and content.

HD number	TIC	T_{eff} (K)	[M/H] (dex)	M (M_{\odot})	R (R_{\odot})	Atmospheric Parameter Source
22349	31852879	4859 ± 132	-0.20 ± 0.30	1.50 ± 0.14	12.18 ± 0.49	5
23128	238180822	4606 ± 92	-0.10 ± 0.25	1.34 ± 0.11	13.50 ± 0.49	5
23381	31960832	4612 ± 92	0.20 ± 0.15	1.45 ± 0.10	12.71 ± 0.31	5
23399	425997943	4816 ± 131	0.30 ± 0.30	1.13 ± 0.16	10.54 ± 0.54	5
...
311740	271795748	4830 ± 97	-0.31 ± 0.24	1.38 ± 0.09	7.61 ± 0.20	5
370635	370115759	4403 ± 88	-0.06 ± 0.05	1.21 ± 0.08	13.63 ± 0.37	1

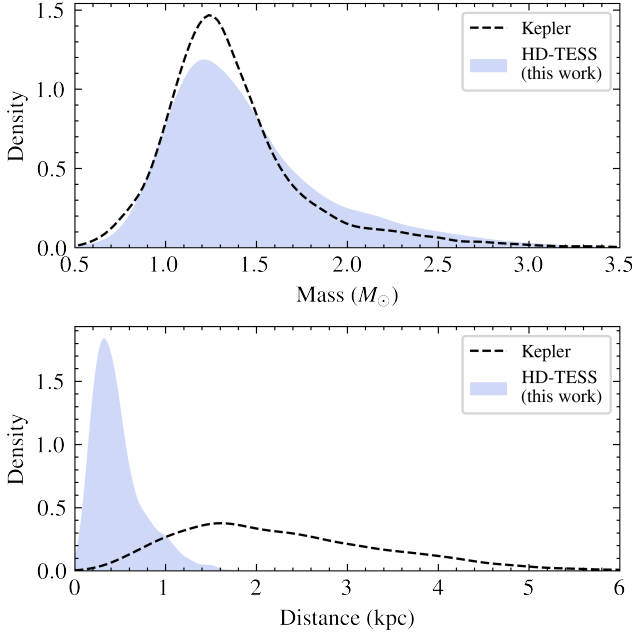


Figure 6. (Top) Kernel density estimates comparing the masses of HD-TESS giants (shaded) with those from a population of giants observed by *Kepler* (Yu et al. 2018). Compared to the *Kepler* giants, our TESS sample has a greater fraction of stars above $1.5M_{\odot}$, which is consistent with comparisons of the seismic mass proxy $\nu_{\text{max}}^{0.75}/\Delta\nu$ between both samples in Figure 4. (Bottom) A comparison of distances between the two giant star samples. TESS probes stellar populations mainly within the solar neighbourhood, whereas *Kepler* probes populations much farther into the Milky Way disk.

for radius, neglecting any potential systematic errors between atmospheric parameter catalogs.

Figure 6 compares the distribution of seismic masses of our TESS giants with those from *Kepler* (Yu et al. 2018) where the TESS sample noticeably contains a greater fraction of stars above $\sim 1.5M_{\odot}$. Such a result is consistent with the comparisons made using purely using the seismic mass proxy in Figure 4, and so these relative mass differences are unlikely to be caused by offsets in temperature and metallicity scales between atmospheric sources. This result suggests that HD-TESS has fractionally more young stars, which is expected of stars in the local neighbourhood for which many have [Fe/H] and [α /Fe] abundances at the solar level (e.g., Haywood et al. 2013; Hayden et al. 2015). The lower panel of Figure 6 shows that the *Kepler* sample comprises more distant stars, many of which belong to older Galactic populations including the thick disk (Silva Aguirre et al. 2018; Miglio et al. 2021) as well as the Galactic halo (Epstein et al. 2014; Mathur et al. 2016).

To establish the differences in masses between the *Kepler* and HD-TESS datasets more concretely, we compare their empirical cumulative distribution functions (ECDFs) in Figure 7. Panel (a1) shows systematic offsets in the between *Kepler* and TESS the seismic mass proxy ECDFs that manifest as a relative overdensity of stars with $1.2M_{\odot} \lesssim M \lesssim 2.2M_{\odot}$ for HD-TESS masses in panel (b1). To include the effects of uncertainties in these comparisons, we apply a Monte-Carlo approach to the D -statistic calculated from the two-sided Kolmogorov-Smirnov test (Massey Jr. 1951). The D -statistic measures the maximum vertical distance between two ECDFs, with larger values generally indicating greater levels of dissimilarity between the two compared datasets. To quantify the impact of our measure-

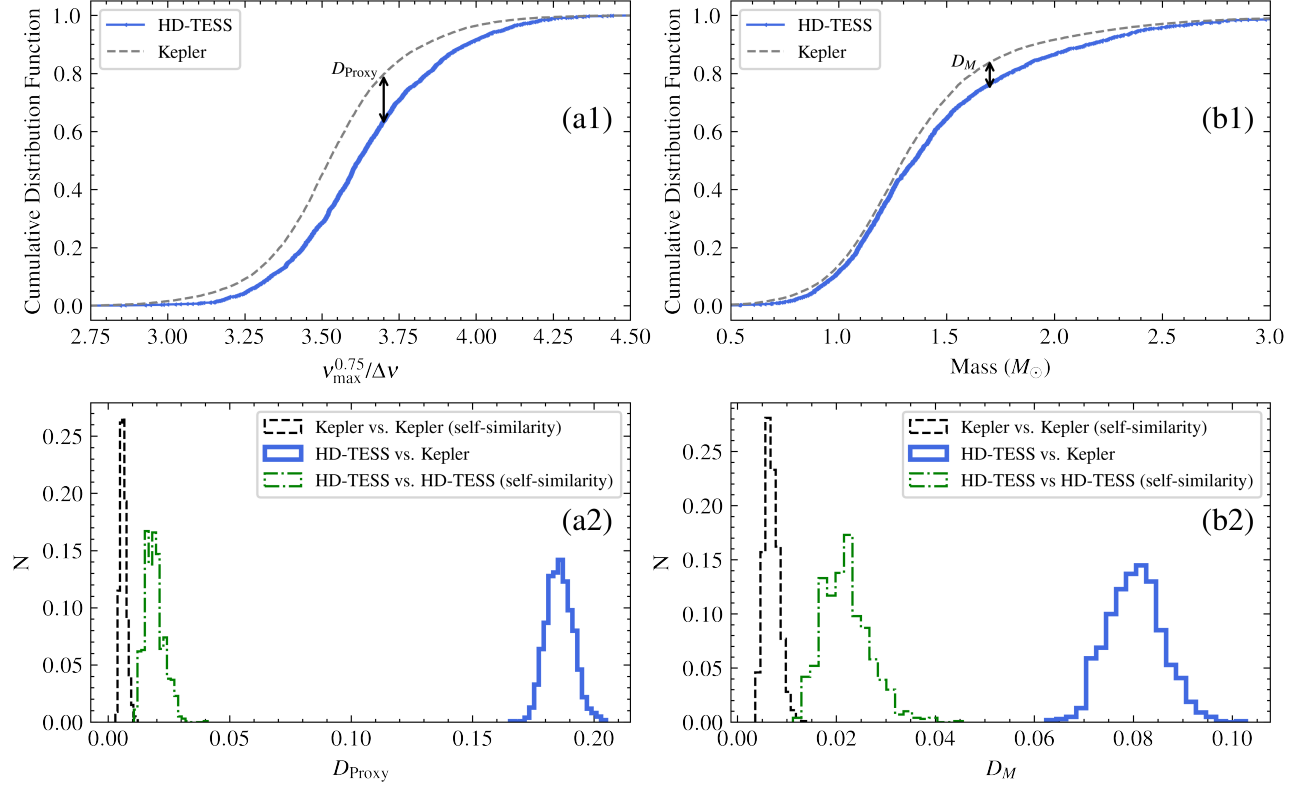


Figure 7. (a1) Empirical cumulative distribution functions (ECDFs) for the HD-TESS and *Kepler* asteroseismic mass proxy values, $\nu_{\max}^{0.75}/\Delta\nu$. The quantity D measures the maximum vertical distance between any two ECDFs. Here, the plotted ECDFs (HD-TESS vs *Kepler*) are constructed using the mean values of ν_{\max} and $\Delta\nu$. (a2) The distribution of D_{Proxy} across 10^5 different noise realizations. The black, dashed histogram is a ‘self-similarity’ D_{Proxy} distribution for the *Kepler* dataset, created by repeatedly comparing one instance of a *Kepler* ECDF to another having a different noise realization. The dash-dotted green histogram is the self-similarity distribution for the HD-TESS dataset. The blue, solid histogram measures similarity *between* HD-TESS and *Kepler* datasets, and its large offset from the other histograms indicates a strong dissimilarity between the underlying *Kepler* and TESS seismic mass proxy distributions that is unlikely to be explained by random uncertainties in *Kepler* or TESS datasets alone. Panels (b1) and (b2) are similar to panels (a1) and (a2), respectively, but for reported values of mass.

ment uncertainties, we first perturb each quantity (seismic mass proxy or stellar mass) from a dataset with its associated uncertainty and construct an instance of its ECDF. A single value of the D -statistic is then computed by comparing this ECDF to another constructed using quantities with another realization of noise or uncertainty. This process is repeated 10^5 times to build up a D -statistic distribution as shown in panels (a2) and (b2) of Figure 7. The ‘*Kepler* vs. *Kepler*’ and ‘HD-TESS vs. HD-TESS’ distributions in these panels are self-similarity distributions. Specifically, these are created by comparing ECDFs of the same dataset (e.g., *Kepler* with itself) but across different noise realizations to show how much variation in the D -statistic is expected from measurement uncertainties alone. Meanwhile, the ‘HD-TESS vs. *Kepler*’ distribution measures similarity between datasets, which shows a large offset compared to the self-similarity distributions. The implication here is that differences in the compared quantities between

HD-TESS and *Kepler* datasets are unlikely caused by measurement uncertainties alone, and we thus conclude that the increase in average mass seen for our TESS dataset relative to *Kepler* is indeed significant.

5. SCIENTIFIC USES FOR THIS CATALOG

Owing to their brightness and intrinsic luminosity, nearby red giants have historically been prime candidates for studies of local stellar populations, such as chemical abundance surveys using high resolution spectroscopy (e.g., Hekker & Meléndez 2007; Luck & Heiter 2007; Luck 2015; Liu et al. 2014; Takeda & Tajitsu 2014) and planet searches using the radial velocity technique (e.g., Döllinger & Hartmann 2021, and references therein). Beyond local surveys, many of these giants have been individually studied for a wide variety of science cases. Figure 8 shows that the number of times some of the brightest targets has been included in a publication ranges in the hundreds, while even for fainter

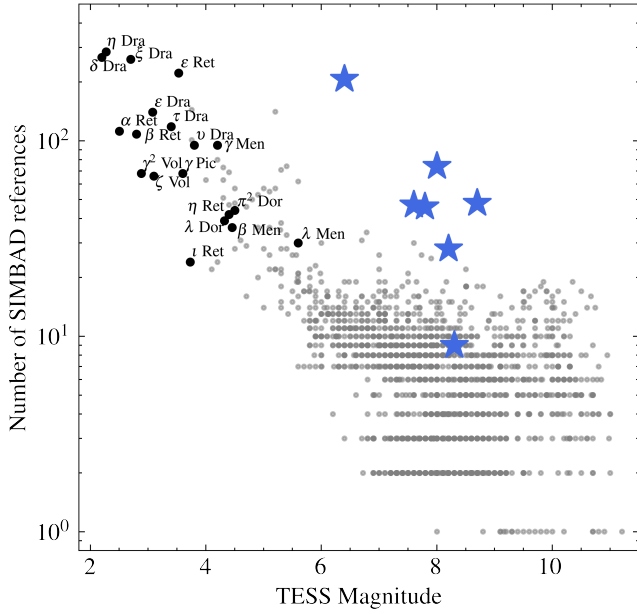


Figure 8. The relative popularity of bright, oscillating red giants in our TESS sample, visualized as the number of references registered on the SIMBAD astronomical database (Wenger et al. 2000) as of January 2022. Bright stars with Bayer designations are annotated in the plot, while blue points indicate interesting giants flagged as ‘peculiar’ by SIMBAD, which here comprises either halo stars or known barium stars (Bidelman & Keenan 1951).

targets there still exists a subset of giants ($T_{\text{mag}} \geq 6$) that are of great interest scientifically. Prior to TESS, however, a vast majority of these giants have not had any precise seismic characterization to complement the studies involving such stars. Although this paper is primarily concerned with assembling a catalog of seismic measurements, we highlight several useful science cases of our catalog unique to bright stars that we will pursue further in future work.

5.1. Stellar Multiplicity

The ever increasing precision of astrometry from the *Gaia* space mission (Gaia Collaboration et al. 2018, 2021) has proven extremely valuable for the study of both resolved (e.g., El-Badry et al. 2019, 2021; Makarov & Fabricius 2021) and unresolved stellar companions (e.g., Belokurov et al. 2020; Penoyre et al. 2022) of nearby stars. Of particular interest are binary systems for which one of its components is an oscillating giant because these enable direct constraints on the age of the co-eval companion. In Figure 9a, we show a cross-match of our TESS sample to the catalog of astrometric binaries from El-Badry et al. (2021), yielding a total of 99 oscillating giants with a low chance alignment probability (< 0.1). Figures 9b-f show that the stars compris-

ing the secondary component in these binary systems span a variety of evolutionary stages based on the color-magnitude diagram, ranging from parts of the main sequence to white dwarfs. Because the giants in our sample generally have well-characterized oscillations, this offers the opportunity of calibrating age relations in other parts of the color-magnitude diagram such as gyrochronology (Skumanich 1972; Barnes 2007), activity indicators along the main sequence (e.g., Pace 2013), and the cooling-age relation for white dwarfs (Winget et al. 1987). These 99 oscillating giants are tabulated in Appendix B.

The orbital solutions of resolved astrometric binaries, measured by methods such as speckle interferometry (e.g., Mason et al. 1999; Balega et al. 2002) or from space astrometry (Makarov & Fabricius 2021; Makarov 2021), provide an estimate of the mass ratio of the binary system. In such scenarios, the availability of precise mass constraints for one component (in this case the red giant primary) for such systems translates into a mass determination of both binary components, which is valuable not only for testing stellar evolution theory, but for estimating masses of stars for which model-independent masses are rare such as subdwarfs and white dwarfs. A cross-match of our sample with the Washington Double Star Catalog (Mason et al. 2022) reveals that 91 of our TESS giants are in known double star systems, while a cross-match with the Fourth Catalog of Interferometric Measurements of Binary Stars (Hartkopf et al. 2001) yields 57 stars with previously measured positions. These are tabulated in Appendix C.

5.2. Benchmarking Asteroseismic Radii with Interferometry

The direct measurement of stellar radii using interferometry provides a powerful, model-independent approach to validate the accuracy of radii inferred using the asteroseismic scaling relations (Huber et al. 2012; White et al. 2015). Given known offsets of masses and radii from asteroseismic scaling relations with respect to stellar models (e.g., Epstein et al. 2014; Sharma et al. 2016) and eclipsing binaries (e.g., Brogaard et al. 2018), it is important that comparisons between interferometric radii with seismic radii be performed across a wide range of metallicities, temperatures, and evolutionary stages. The bottleneck, however, has been the availability of precise seismic data for interferometric targets, for which to date only 7 giants with $R \geq 3R_{\odot}$ has had published joint seismic-interferometric coverage (Huber et al. 2012; Johnson et al. 2014; Beck et al. 2015). The HD-TESS catalog can significantly alleviate this limi-

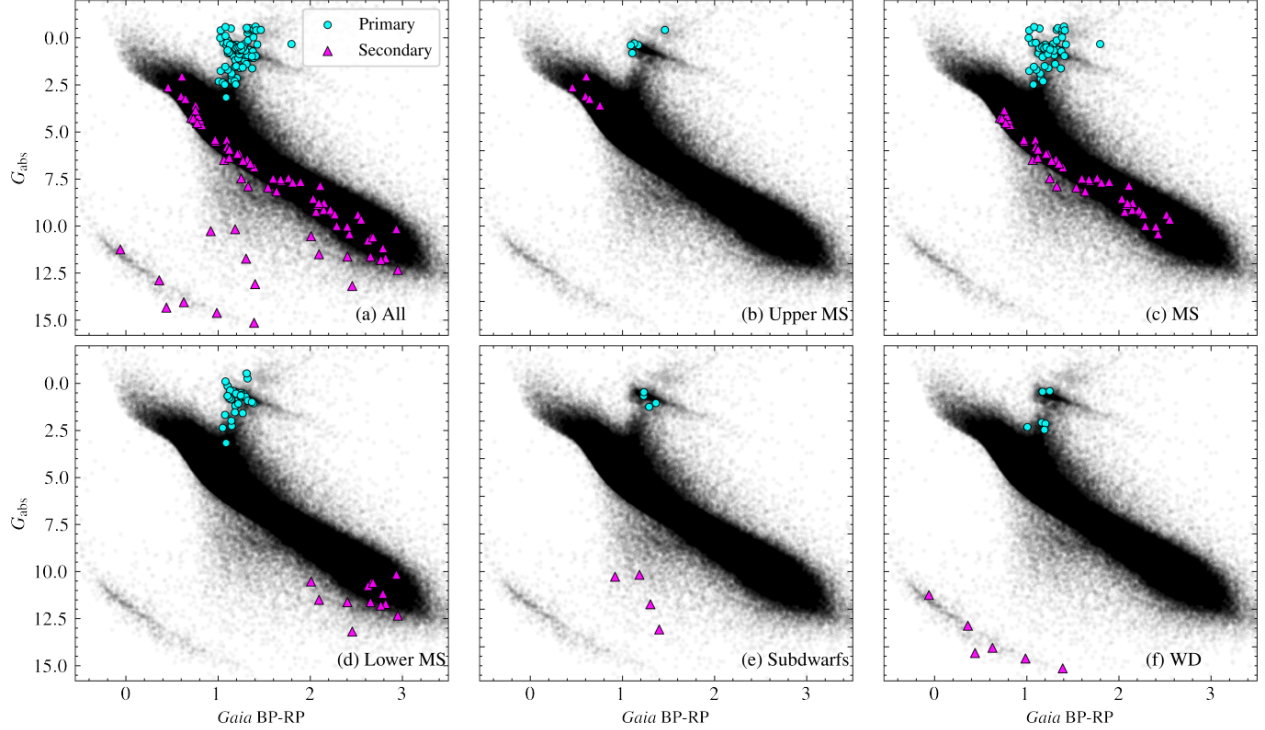


Figure 9. *Gaia* color-magnitude diagrams showing the 99 oscillating giants in our sample known to be astrometric binaries from the El-Badry et al. (2021) catalog. Only binary systems that have a chance alignment probability less than 0.1 from the catalog are identified. The blue points mark the brighter, primary component (oscillating giant) of each binary system, while the magenta points mark the corresponding fainter, secondary component. The black points are a random subset of stars from *Gaia* EDR3 (Gaia Collaboration et al. 2021). Panel (a) shows all identified binary systems, which are further categorized in panels (b-f) based on the location of their secondary components in the color-magnitude diagram: (b) on the upper main sequence (MS); (c) on the main sequence; (d) on the lower main sequence; (e) in the subdwarf regime; (f) along the white dwarf (WD) sequence.

tation by providing a large quantity of bright targets amenable to both asteroseismology and interferometry.

Figure 10 compares radii for 16 red giants with published interferometric measurements — a factor of two increase from literature. The power spectrum and seismic measurements for each of these 16 giants is presented in Appendix D. The interferometric radii from each literature study (Baines et al. 2010, 2011, 2016, 2018, Ligi et al. 2016, von Braun & Boyajian 2017¹, White et al. 2018, Karovicova et al. 2020) are computed by combining reported limb darkened angular diameters with parallaxes from *Gaia* EDR3. In Appendix E, we perform the same analysis as in this Section using interferometric radii derived but using Hipparcos parallaxes (van Leeuwen 2007), where we generally find worse agreement. We thus use *Gaia* EDR3 parallaxes for the

rest of the analysis presented here. We correct for potential zero-point offsets in the parallaxes following Lindgren et al. (2020) and the correction recommended by Zinn (2021).

Three comparisons are presented in Figure 10: (a) Using the Sharma et al. (2016) correction, which provides a $f_{\Delta\nu}$ dependent on the T_{eff} , $[\text{Fe}/\text{H}]$, and evolutionary state of each star reported in this work; (b) No corrections (i.e., $f_{\Delta\nu} = 1$) with the adopted T_{eff} in this work, (c) No corrections and using the T_{eff} reported from each interferometric study. The latter comparison is made in the interest of consistency as the quoted literature T_{eff} values are typically derived using angular diameters through an application of the Stefan-Boltzmann law. We observe the following:

- The application of a star-dependent correction factor $f_{\Delta\nu}$ generally improves the agreement between seismic and interferometric radii, especially for low-luminosity giants with $R \lesssim 15R_{\odot}$. In particular, we find the median fractional difference between the corrected seismic radii and interferometric to be approximately at the $3.2 \pm 1.7\%$

¹ The following stars reported by von Braun & Boyajian (2017) have reported angular diameters that are weighted averages of other literature values: HD 27256 — Cusano et al. (2012); HD 148387 — Nordgren et al. (2001); HD 180711 — Nordgren et al. (2001); Mozurkewich et al. (2003).

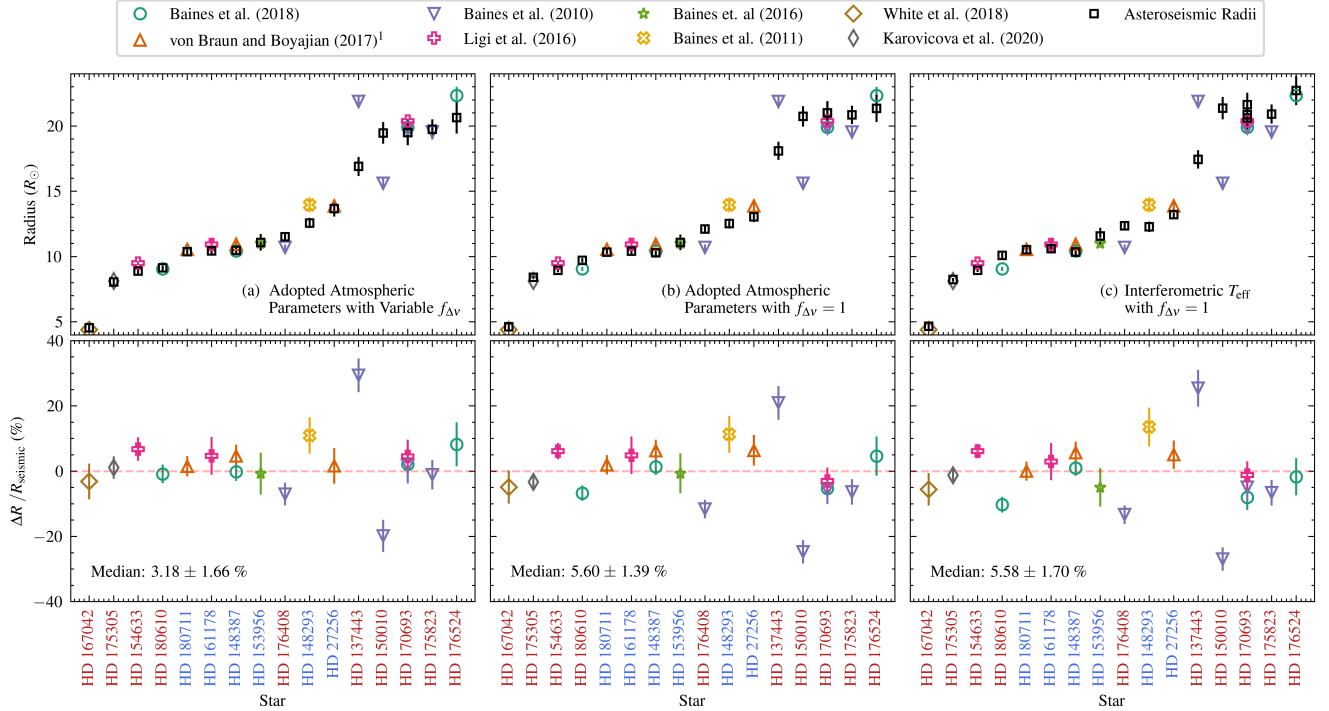


Figure 10. Comparisons of radii from the asteroseismic scaling relations with linear radii from interferometry across literature for 16 oscillating giants from the HD-TESS catalog. The lower panels show fractional difference between radii estimates, where $\Delta R = R_{\text{interferometric}} - R_{\text{seismic}}$. The median $\Delta R/R_{\text{seismic}}$ for each comparison is quoted in each lower panel, with standard errors as the reported uncertainty. The color of each star’s label along the x-axis reflects its evolutionary state, with red for RGB and blue for CHeB. (a) R_{seismic} uses $(T_{\text{eff}}, [M/H])$ adopted in this study and applies the Sharma et al. (2016) correction to compute the correction factor $f_{\Delta\nu}$ (see Equation 2). (b) R_{seismic} uses T_{eff} values adopted in this work, with $f_{\Delta\nu} = 1$. (c) R_{seismic} uses the literature (i.e., interferometric) T_{eff} values reported from each cited work, with $f_{\Delta\nu} = 1$.

level. In contrast, the use of no correction factor in Figures 10b-c result in greater median fractional differences ($\sim 5 - 6\%$). These findings are in accordance with other benchmark studies of asteroseismic radii using *Gaia* parallaxes (Zinn et al. 2019) as well as using dynamical radii from eclipsing binaries (Gaulme et al. 2016; Brogaard et al. 2018; Kallinger et al. 2018), and further confirms that a correction factor to the asteroseismic scaling relations is indeed warranted.

- The similarity of trends between panels (b) and (c) suggests that the improvements seen in (a) are mostly from the adoption of a star-dependent $f_{\Delta\nu}$, rather than by differences in the adopted effective temperatures (spectroscopic versus interferometric). Regardless of the adopted effective temperature, scenarios (b) and (c), which do not adopt a star-dependent $f_{\Delta\nu}$, show larger discrepancies compared to the opposite scenario in (a). This implies that the presence of any form of $f_{\Delta\nu}$ is better than no correction whatsoever.

- The two most discrepant stars, HD 137443 and HD 150010, are labelled as ‘RGB’ stars with a measured $\nu_{\text{max}} \sim 10 - 15 \mu\text{Hz}$. It is thus plausible that these are actually helium shell-burning asymptotic giant branch (AGB) stars, which are generally difficult to disentangle from hydrogen shell-burning RGB stars seismically (e.g., Stello et al. 2013, their Figure 4b, Dréau et al. 2021). The Sharma et al. (2016) correction does not yet account for evolutionary stages past core-helium burning, which may explain the large observed differences between seismic and interferometric radii. We note, however, that the interferometry for these stars are only based on only a single series of measurements by Baines et al. (2010), and thus could be affected by instrument-dependent systematics in angular diameter measurements (Tayar et al. 2022).

6. CONCLUSIONS

Our main conclusions are as follows:

1. We present a catalog of fundamental asteroseismic parameters $\Delta\nu$ and ν_{max} and evolutionary states for 1,709 bright, oscillating red giants from the

Henry Draper Catalog. These stars are required to have been observed for at least 6 months within one TESS observing cycle throughout Cycles 1-3 and thus are located near the TESS continuous viewing zones.

2. We provide seismic mass (κ_M) and radius (κ_R) coefficients for users that wish to use their own effective temperatures and metallicities when applying the asteroseismic scaling relations to estimate masses and radii. With the application of such scaling relations, we determine masses with a typical precision of 8.3% and radii with a typical precision of 3.2% for the stars in our sample using a compilation of atmospheric parameters from literature. Compared to the population of *Kepler* red giants, the HD-TESS sample is systematically more massive, with a larger fraction of stars having $M \gtrsim 1.5M_\odot$.
3. 99 stars in our sample are known astrometric binaries from *Gaia* EDR3, while 40 are well-known visual binaries with archival measurements from the Washington Double Star catalog. These binaries include those with subdwarfs and white dwarfs as the secondary.
4. We benchmark radii from asteroseismic scaling relations against radii measured using interferometry for 16 giants in our sample. Our results show that the median fractional difference between

the two radii are approximately 3% for giants with $R < 15R_\odot$ when calculating interferometric radii using *Gaia* parallaxes. Reaching this level of agreement between the two approaches, however, requires a correction factor to the scaling relations, in agreement with other independent benchmarking studies.

The preliminary work here highlights the value of TESS observations in calibrating methods of inferring fundamental stellar parameters of well-studied bright stars. The large number of precise seismic measurements from this work, which when combined with accurate *Gaia* parallaxes and ground-based spectroscopy, will allow more frequent and consistent benchmarks of asteroseismic inference methods against interferometry. Neither the highlighted science cases nor the seismic measurements provided in this work are exhaustive in nature. As TESS pursues further observing cycles, not only will the asteroseismic precision of frequently visited regions of the sky increase, but more bright stars near us — particularly those closer to the ecliptic plane — will also eventually be accessible with precision asteroseismology. In that sense, the work presented here acts as a precursor for a more comprehensive asteroseismic catalog of bright stars in the near future, where we will aim for a much more extensive sky coverage.

Facilities: TESS

APPENDIX

A. FREQUENCY AT MAXIMUM POWER FOR 2,611 OSCILLATING GIANTS

Table A1 lists the ν_{\max} measurements for 2,611 oscillating giants from the HD catalog that show oscillations in this work. The table entries comprise the 1,709 stars forming the main HD-TESS catalog (Table 1) as well as 903 additional red giants whose $\Delta\nu$ cannot be measured in this study.

B. SPATIALLY RESOLVED ASTROMETRIC BINARIES FROM *GAIA* EDR3

Table B1 lists the 99 oscillating giants in our sample that have been identified as being part of an astrometric binary system in the El-Badry et al. (2021) catalog. From the cross-match, we select only binaries with a computed chance alignment probability less than 0.1.

C. DOUBLE STARS AND INTERFEROMETRIC BINARIES

Table C1 lists a cross-match of our oscillating giant sample to the Washington Double Star catalog (Mason et al. 2022). Table C2 presents a cross-match to the Fourth Catalog of Interferometric Measurements of Binary Stars (Hartkopf et al. 2001). The full version of both tables are available in a machine-readable format in the online journal, with a portion shown here for guidance regarding their form and content.

Table A1. The measured frequency of maximum power, ν_{\max} of 2,611 giants with detected oscillations in this work. Each star’s identifier in the Henry Draper (HD) catalog and the TESS Input Catalog (TIC) is provided. The full version of this table is available in a machine-readable format in the online journal, with a portion shown here for guidance regarding its form and content.

HD number	TIC identifier	ν_{\max} μHz
22349	31852879	34.04 ± 0.50
23128	238180822	25.24 ± 0.39
23253	31959761	55.80 ± 1.25
23266	311925612	28.29 ± 0.75
...
311763	272472375	18.67 ± 1.50
370635	370115759	22.95 ± 0.35

Table B1. List of 99 binaries from the [El-Badry et al. \(2021\)](#) catalog for which the primary is an oscillating giant in our sample. The quoted *Gaia* source IDs are those from Early Data Release 3 ([Gaia Collaboration et al. 2021](#)). The full version of this table is available in a machine-readable format in the online journal, with a portion shown here for guidance regarding its form and content.

HD number	Primary Source ID	Secondary Source ID
24272	4667870070470785792	4667870070470786816
27068	4676770239141111424	4676770239141111040
27670	4676012709989349376	4676012778708825344
28633	4656569496121672832	4656569461761934592
...
311373	5215069141868112256	5215069141868555648
311734	5263024685110990720	5263024685110990592

D. POWER SPECTRA OF OSCILLATING GIANTS WITH INTERFEROMETRY

Figure 11 shows the échelle diagram and power spectra of the 16 oscillating red giants with interferometric radii discussed in Section 5.2.

E. SEISMIC RADII VERSUS INTERFEROMETRIC RADII COMPUTED USING HIPPARCOS PARALLAXES

Figure 12 repeats the analysis in Section 5.2 but uses interferometric radii derived from Hipparcos ([van Leeuwen 2007](#)) parallaxes instead of *Gaia* EDR3. The results shown here do not change the conclusions from Section 5.2; however the overall worse agreement suggests that *Gaia* parallaxes are more accurate as well as more precise for the giants analyzed in this study.

Table C1. List of 91 oscillating giants that are known double stars in the Washington Double Star (WDS) Catalog.

HD number	WDS identifier
23817	WDS J03442-6448A
24461	WDS J03480-7048A
25106	WDS J03549-6627AB
27256	WDS J04144-6228A
...	...
239229	WDS J19490+5916A
269894	WDS J05385-7045AB

Table C2. List of 57 oscillating giants with archival position measurements from the Fourth Catalog of Interferometric Measurements of Binary Stars.

HD number	TIC ID
132464	219018004
132698	288185404
137292	219731897
141264	272746493
...	
238629	199713797
270011	389325554

REFERENCES

- Abdurro’uf, Accetta, K., Aerts, C., et al. 2022, ApJS, 259, 35, doi: [10.3847/1538-4365/ac4414](https://doi.org/10.3847/1538-4365/ac4414)
- Addison, B., Wright, D. J., Wittenmyer, R. A., et al. 2019, PASP, 131, 115003, doi: [10.1088/1538-3873/ab03aa](https://doi.org/10.1088/1538-3873/ab03aa)
- Anders, F., Khalatyan, A., Queiroz, A. B. A., et al. 2022, A&A, 658, A91, doi: [10.1051/0004-6361/202142369](https://doi.org/10.1051/0004-6361/202142369)
- Baglin, A., Auvergne, M., Barge, P., et al. 2009, in Transiting Planets, ed. F. Pont, D. Sasselov, & M. J. Holman, Vol. 253, 71–81, doi: [10.1017/S1743921308026252](https://doi.org/10.1017/S1743921308026252)
- Baines, E. K., Armstrong, J. T., Schmitt, H. R., et al. 2018, AJ, 155, 30, doi: [10.3847/1538-3881/aa9d8b](https://doi.org/10.3847/1538-3881/aa9d8b)
- Baines, E. K., Döllinger, M. P., Guenther, E. W., et al. 2016, AJ, 152, 66, doi: [10.3847/0004-6256/152/3/66](https://doi.org/10.3847/0004-6256/152/3/66)
- Baines, E. K., Döllinger, M. P., Cusano, F., et al. 2010, ApJ, 710, 1365, doi: [10.1088/0004-637X/710/2/1365](https://doi.org/10.1088/0004-637X/710/2/1365)
- Baines, E. K., McAlister, H. A., ten Brummelaar, T. A., et al. 2011, ApJ, 731, 132, doi: [10.1088/0004-637X/731/2/132](https://doi.org/10.1088/0004-637X/731/2/132)
- Balega, I. I., Balega, Y. Y., Hofmann, K. H., et al. 2002, A&A, 385, 87, doi: [10.1051/0004-6361:20020005](https://doi.org/10.1051/0004-6361:20020005)
- Barnes, S. A. 2007, ApJ, 669, 1167, doi: [10.1086/519295](https://doi.org/10.1086/519295)
- Beck, P. G., Kambe, E., Hillen, M., et al. 2015, A&A, 573, A138, doi: [10.1051/0004-6361/201323019](https://doi.org/10.1051/0004-6361/201323019)

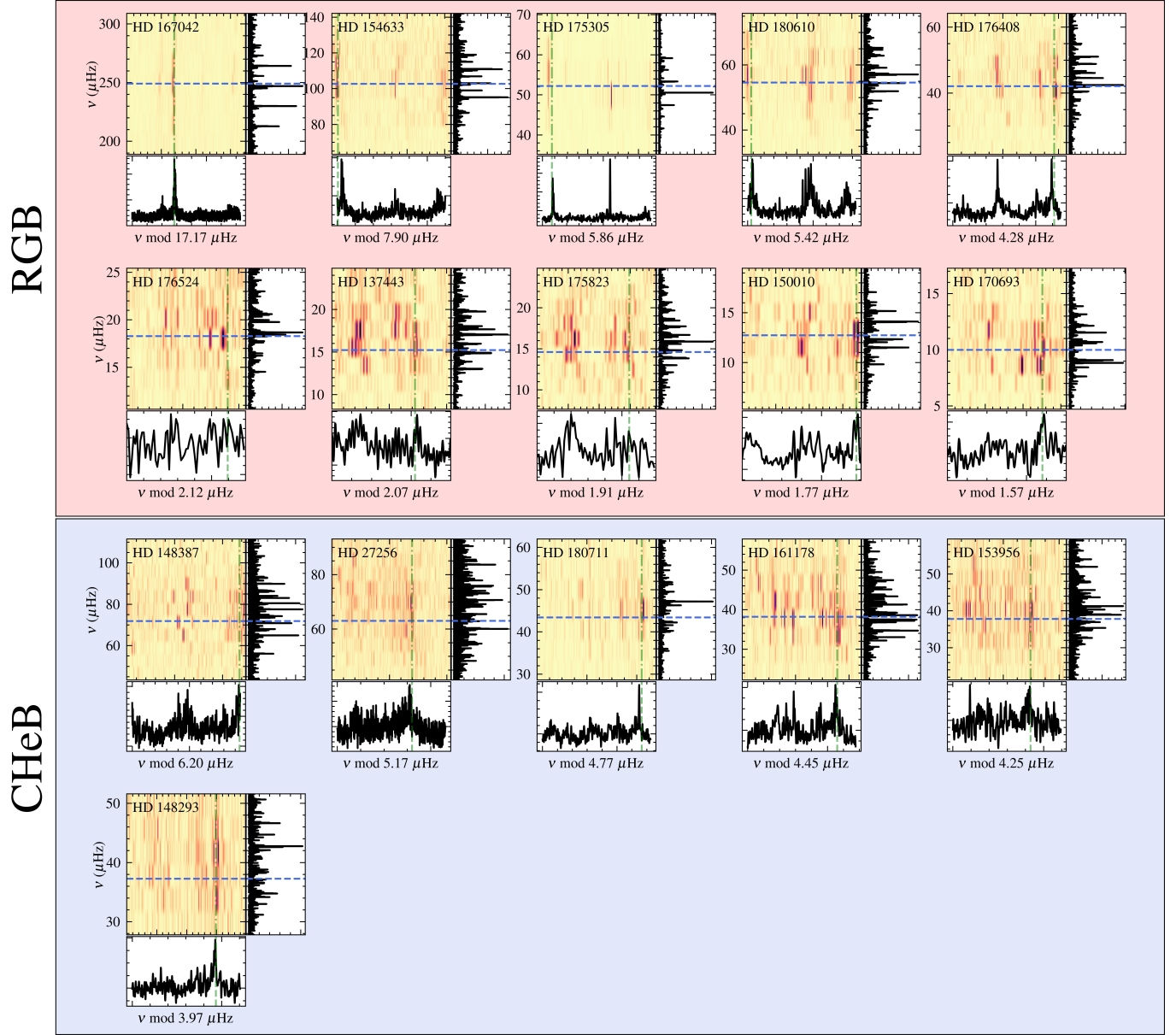


Figure 11. Seismic visual diagnostic plots for the 16 oscillating giants benchmarked against interferometric measurements in Section 5.2, categorized by their evolutionary state (RGB = hydrogen shell-burning, CHeB = core helium-burning). The stars are ordered in decreasing $\Delta\nu$ from the top left to the bottom right in each category. The blue horizontal line in each panel corresponds to ν_{\max} , while the green vertical line corresponds to the location of the radial mode-ridge in the échelle diagrams.

Bedding, T. R. 2014, in *Asteroseismology*, ed. P. L. Pallé & C. Esteban, 60

Bedding, T. R., Mosser, B., Huber, D., et al. 2011, *Nature*, 471, 608, doi: [10.1038/nature09935](https://doi.org/10.1038/nature09935)

Belkacem, K., Goupil, M. J., Dupret, M. A., et al. 2011, *A&A*, 530, A142, doi: [10.1051/0004-6361/201116490](https://doi.org/10.1051/0004-6361/201116490)

Belokurov, V., Penoyre, Z., Oh, S., et al. 2020, *MNRAS*, 496, 1922, doi: [10.1093/mnras/staa1522](https://doi.org/10.1093/mnras/staa1522)

Bidelman, W. P., & Keenan, P. C. 1951, *ApJ*, 114, 473, doi: [10.1086/145488](https://doi.org/10.1086/145488)

Borucki, W. J., Koch, D., Basri, G., et al. 2010, *Science*, 327, 977, doi: [10.1126/science.1185402](https://doi.org/10.1126/science.1185402)

Brogaard, K., Hansen, C. J., Miglio, A., et al. 2018, *MNRAS*, 476, 3729, doi: [10.1093/mnras/sty268](https://doi.org/10.1093/mnras/sty268)

Brown, T. M., Gilliland, R. L., Noyes, R. W., & Ramsey, L. W. 1991, *ApJ*, 368, 599, doi: [10.1086/169725](https://doi.org/10.1086/169725)

Cannon, A. J., & Pickering, E. C. 1993, *VizieR Online Data Catalog*, III/135A

Chaplin, W. J., Basu, S., Huber, D., et al. 2014, *ApJS*, 210, 1, doi: [10.1088/0067-0049/210/1/1](https://doi.org/10.1088/0067-0049/210/1/1)

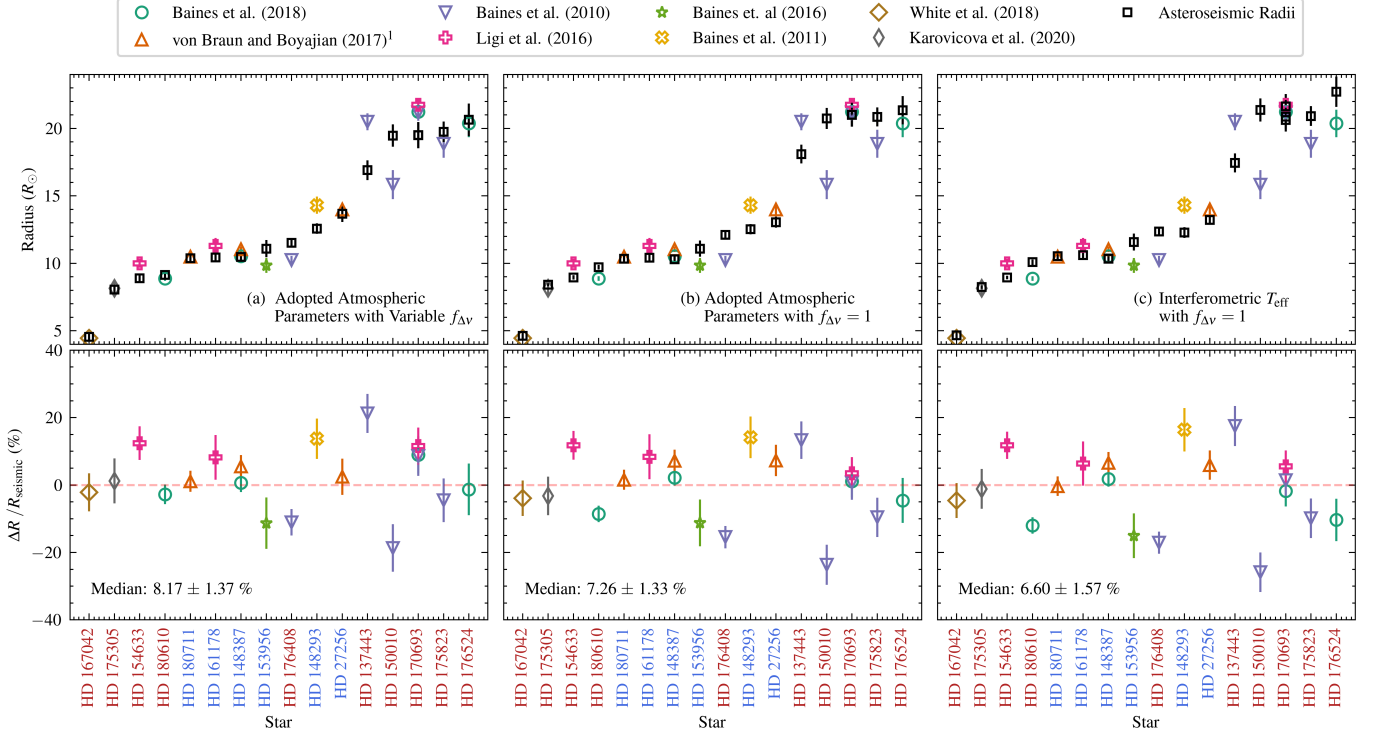


Figure 12. Comparisons of radii from the asteroseismic scaling relations with linear radii from interferometry across literature for 16 oscillating giants from our TESS giant sample. This Figure is identical to Figure 10, except that the inteferometric radii are derived using Hipparcos parallaxes as opposed to *Gaia* EDR3 parallaxes.

Charbonnel, C., Lagarde, N., Jasiewicz, G., et al. 2020, *A&A*, 633, A34, doi: [10.1051/0004-6361/201936360](https://doi.org/10.1051/0004-6361/201936360)

Christensen-Dalsgaard, J. 1984, in *Space Research in Stellar Activity and Variability*, ed. A. Manganey & F. Praderie, 11

Christensen-Dalsgaard, J. 2015, *MNRAS*, 453, 666, doi: [10.1093/mnras/stv1656](https://doi.org/10.1093/mnras/stv1656)

Colman, I. L., Huber, D., Bedding, T. R., et al. 2017, *MNRAS*, 469, 3802, doi: [10.1093/mnras/stx1056](https://doi.org/10.1093/mnras/stx1056)

Cusano, F., Paladini, C., Richichi, A., et al. 2012, *A&A*, 539, A58, doi: [10.1051/0004-6361/201116731](https://doi.org/10.1051/0004-6361/201116731)

Döllinger, M. P., & Hartmann, M. 2021, *ApJS*, 256, 10, doi: [10.3847/1538-4365/ac081a](https://doi.org/10.3847/1538-4365/ac081a)

Dréau, G., Mosser, B., Lebreton, Y., Gehan, C., & Kallinger, T. 2021, *A&A*, 650, A115, doi: [10.1051/0004-6361/202040240](https://doi.org/10.1051/0004-6361/202040240)

El-Badry, K., Rix, H.-W., & Heintz, T. M. 2021, *MNRAS*, 506, 2269, doi: [10.1093/mnras/stab323](https://doi.org/10.1093/mnras/stab323)

El-Badry, K., Rix, H.-W., Tian, H., Duchêne, G., & Moe, M. 2019, *MNRAS*, 489, 5822, doi: [10.1093/mnras/stz2480](https://doi.org/10.1093/mnras/stz2480)

Epstein, C. R., Elsworth, Y. P., Johnson, J. A., et al. 2014, *ApJL*, 785, L28, doi: [10.1088/2041-8205/785/2/L28](https://doi.org/10.1088/2041-8205/785/2/L28)

Feillet, D. K., Bovy, J., Holtzman, J., et al. 2018, *MNRAS*, 477, 2326, doi: [10.1093/mnras/sty779](https://doi.org/10.1093/mnras/sty779)

Frandsen, S., Carrier, F., Aerts, C., et al. 2002, *A&A*, 394, L5, doi: [10.1051/0004-6361:20021281](https://doi.org/10.1051/0004-6361:20021281)

Gaia Collaboration, Brown, A. G. A., Vallenari, A., et al. 2018, *A&A*, 616, A1, doi: [10.1051/0004-6361/201833051](https://doi.org/10.1051/0004-6361/201833051)

—. 2021, *A&A*, 649, A1, doi: [10.1051/0004-6361/202039657](https://doi.org/10.1051/0004-6361/202039657)

García, R. A., & Stello, D. 2015, in *Extraterrestrial Seismology*, 159–169, doi: [10.1017/CBO9781107300668.014](https://doi.org/10.1017/CBO9781107300668.014)

Gaulme, P., McKeever, J., Jackiewicz, J., et al. 2016, *ApJ*, 832, 121, doi: [10.3847/0004-637X/832/2/121](https://doi.org/10.3847/0004-637X/832/2/121)

Hall, O. J., Davies, G. R., Elsworth, Y. P., et al. 2019, *MNRAS*, 486, 3569, doi: [10.1093/mnras/stz1092](https://doi.org/10.1093/mnras/stz1092)

Hartkopf, W. I., McAlister, H. A., & Mason, B. D. 2001, *AJ*, 122, 3480, doi: [10.1086/323923](https://doi.org/10.1086/323923)

Hayden, M. R., Bovy, J., Holtzman, J. A., et al. 2015, *ApJ*, 808, 132, doi: [10.1088/0004-637X/808/2/132](https://doi.org/10.1088/0004-637X/808/2/132)

Haywood, M., Di Matteo, P., Lehnert, M. D., Katz, D., & Gómez, A. 2013, *A&A*, 560, A109, doi: [10.1051/0004-6361/201321397](https://doi.org/10.1051/0004-6361/201321397)

Hekker, S., & Christensen-Dalsgaard, J. 2017, *A&A Rv*, 25, 1, doi: [10.1007/s00159-017-0101-x](https://doi.org/10.1007/s00159-017-0101-x)

Hekker, S., & Meléndez, J. 2007, *A&A*, 475, 1003, doi: [10.1051/0004-6361:20078233](https://doi.org/10.1051/0004-6361:20078233)

Hon, M., Stello, D., García, R. A., et al. 2019, *MNRAS*, 485, 5616, doi: [10.1093/mnras/stz622](https://doi.org/10.1093/mnras/stz622)

- Hon, M., Stello, D., & Yu, J. 2017, *MNRAS*, 469, 4578, doi: [10.1093/mnras/stx1174](https://doi.org/10.1093/mnras/stx1174)
- . 2018, *MNRAS*, 476, 3233, doi: [10.1093/mnras/sty483](https://doi.org/10.1093/mnras/sty483)
- Hon, M., Huber, D., Kuszlewicz, J. S., et al. 2021, *ApJ*, 919, 131, doi: [10.3847/1538-4357/ac14b1](https://doi.org/10.3847/1538-4357/ac14b1)
- Howell, S. B., Sobeck, C., Haas, M., et al. 2014, *PASP*, 126, 398, doi: [10.1086/676406](https://doi.org/10.1086/676406)
- Huang, C. X., Vanderburg, A., Pál, A., et al. 2020a, *Research Notes of the American Astronomical Society*, 4, 204, doi: [10.3847/2515-5172/abca2e](https://doi.org/10.3847/2515-5172/abca2e)
- . 2020b, *Research Notes of the American Astronomical Society*, 4, 206, doi: [10.3847/2515-5172/abca2d](https://doi.org/10.3847/2515-5172/abca2d)
- Huber, D., Stello, D., Bedding, T. R., et al. 2009, *Communications in Asteroseismology*, 160, 74, <https://arxiv.org/abs/0910.2764>
- Huber, D., Bedding, T. R., Stello, D., et al. 2011, *ApJ*, 743, 143, doi: [10.1088/0004-637X/743/2/143](https://doi.org/10.1088/0004-637X/743/2/143)
- Huber, D., Ireland, M. J., Bedding, T. R., et al. 2012, *ApJ*, 760, 32, doi: [10.1088/0004-637X/760/1/32](https://doi.org/10.1088/0004-637X/760/1/32)
- Huber, D., Chaplin, W. J., Christensen-Dalsgaard, J., et al. 2013, *ApJ*, 767, 127, doi: [10.1088/0004-637X/767/2/127](https://doi.org/10.1088/0004-637X/767/2/127)
- Huber, D., Zinn, J., Bojsen-Hansen, M., et al. 2017, *ApJ*, 844, 102, doi: [10.3847/1538-4357/aa75ca](https://doi.org/10.3847/1538-4357/aa75ca)
- Jenkins, J. M. 2020, *Kepler Data Processing Handbook: Overview of the Science Operations Center*, id. 2, Kepler Science Document KSCI-19081-003
- Jofré, P., Heiter, U., Tucci Maia, M., et al. 2018, *Research Notes of the American Astronomical Society*, 2, 152, doi: [10.3847/2515-5172/aadc61](https://doi.org/10.3847/2515-5172/aadc61)
- Johnson, J. A., Huber, D., Boyajian, T., et al. 2014, *ApJ*, 794, 15, doi: [10.1088/0004-637X/794/1/15](https://doi.org/10.1088/0004-637X/794/1/15)
- Kallinger, T., Beck, P. G., Stello, D., & Garcia, R. A. 2018, *A&A*, 616, A104, doi: [10.1051/0004-6361/201832831](https://doi.org/10.1051/0004-6361/201832831)
- Kallinger, T., Mosser, B., Hekker, S., et al. 2010, *A&A*, 522, A1, doi: [10.1051/0004-6361/201015263](https://doi.org/10.1051/0004-6361/201015263)
- Karovicova, I., White, T. R., Nordlander, T., et al. 2020, *A&A*, 640, A25, doi: [10.1051/0004-6361/202037590](https://doi.org/10.1051/0004-6361/202037590)
- Khan, S., Hall, O. J., Miglio, A., et al. 2018, *ApJ*, 859, 156, doi: [10.3847/1538-4357/aabf90](https://doi.org/10.3847/1538-4357/aabf90)
- Kjeldsen, H., Bedding, T. R., Viskum, M., & Frandsen, S. 1995, *AJ*, 109, 1313, doi: [10.1086/117363](https://doi.org/10.1086/117363)
- Kunimoto, M., Huang, C., Tey, E., et al. 2021, *Research Notes of the American Astronomical Society*, 5, 234, doi: [10.3847/2515-5172/ac2ef0](https://doi.org/10.3847/2515-5172/ac2ef0)
- Li, T., Li, Y., Bi, S., et al. 2022, *ApJ*, 927, 167, doi: [10.3847/1538-4357/ac4fbf](https://doi.org/10.3847/1538-4357/ac4fbf)
- Li, Y., Bedding, T. R., Stello, D., et al. 2021, *MNRAS*, 501, 3162, doi: [10.1093/mnras/staa3932](https://doi.org/10.1093/mnras/staa3932)
- Ligi, R., Creevey, O., Mourard, D., et al. 2016, *A&A*, 586, A94, doi: [10.1051/0004-6361/201527054](https://doi.org/10.1051/0004-6361/201527054)
- Lindgren, L., Klioner, S. A., Hernández, J., et al. 2020, *arXiv e-prints*, arXiv:2012.03380, <https://arxiv.org/abs/2012.03380>
- Liu, Y. J., Tan, K. F., Wang, L., et al. 2014, *ApJ*, 785, 94, doi: [10.1088/0004-637X/785/2/94](https://doi.org/10.1088/0004-637X/785/2/94)
- Luck, R. E. 2015, *AJ*, 150, 88, doi: [10.1088/0004-6256/150/3/88](https://doi.org/10.1088/0004-6256/150/3/88)
- Luck, R. E., & Heiter, U. 2007, *AJ*, 133, 2464, doi: [10.1086/513194](https://doi.org/10.1086/513194)
- Mackereth, J. T., Miglio, A., Elsworth, Y., et al. 2021, *MNRAS*, 502, 1947, doi: [10.1093/mnras/stab098](https://doi.org/10.1093/mnras/stab098)
- Makarov, V. V. 2021, *RMxAA*, 57, 399, doi: [10.22201/ia.01851101p.2021.57.02.12](https://doi.org/10.22201/ia.01851101p.2021.57.02.12)
- Makarov, V. V., & Fabricius, C. 2021, *AJ*, 162, 260, doi: [10.3847/1538-3881/ac2ee0](https://doi.org/10.3847/1538-3881/ac2ee0)
- Malla, S. P., Stello, D., Huber, D., et al. 2020, *MNRAS*, 496, 5423, doi: [10.1093/mnras/staa1793](https://doi.org/10.1093/mnras/staa1793)
- Mason, B. D., Douglass, G. G., & Hartkopf, W. I. 1999, *AJ*, 117, 1023, doi: [10.1086/300748](https://doi.org/10.1086/300748)
- Mason, B. D., Wycoff, G. L., Hartkopf, W. I., Douglass, G. G., & Worley, C. E. 2001, *AJ*, 122, 3466, doi: [10.1086/323920](https://doi.org/10.1086/323920)
- . 2022, *VizieR Online Data Catalog*, B/wds
- Massey Jr., F. J. 1951, *Journal of the American Statistical Association*, 46, 68, doi: [10.1080/01621459.1951.10500769](https://doi.org/10.1080/01621459.1951.10500769)
- Mathur, S., García, R. A., Huber, D., et al. 2016, *ApJ*, 827, 50, doi: [10.3847/0004-637X/827/1/50](https://doi.org/10.3847/0004-637X/827/1/50)
- McAlister, H. A. 1977, *ApJ*, 215, 159, doi: [10.1086/155343](https://doi.org/10.1086/155343)
- Miglio, A., Montalbán, J., Baudin, F., et al. 2009, *A&A*, 503, L21, doi: [10.1051/0004-6361/200912822](https://doi.org/10.1051/0004-6361/200912822)
- Miglio, A., Chiappini, C., Mackereth, J. T., et al. 2021, *A&A*, 645, A85, doi: [10.1051/0004-6361/202038307](https://doi.org/10.1051/0004-6361/202038307)
- Mosser, B., Michel, E., Samadi, R., et al. 2019, *A&A*, 622, A76, doi: [10.1051/0004-6361/201834607](https://doi.org/10.1051/0004-6361/201834607)
- Mozurkewich, D., Armstrong, J. T., Hindsley, R. B., et al. 2003, *AJ*, 126, 2502, doi: [10.1086/378596](https://doi.org/10.1086/378596)
- Nesterov, V. V., Kuzmin, A. V., Ashimbaeva, N. T., et al. 1995, *A&AS*, 110, 367
- Nordgren, T. E., Sudol, J. J., & Mozurkewich, D. 2001, *AJ*, 122, 2707, doi: [10.1086/323546](https://doi.org/10.1086/323546)
- Pace, G. 2013, *A&A*, 551, L8, doi: [10.1051/0004-6361/201220364](https://doi.org/10.1051/0004-6361/201220364)
- Penoyre, Z., Belokurov, V., & Evans, N. W. 2022, *arXiv e-prints*, arXiv:2202.06963, <https://arxiv.org/abs/2202.06963>
- Pepe, F., Lovis, C., Ségransan, D., et al. 2011, *A&A*, 534, A58, doi: [10.1051/0004-6361/201117055](https://doi.org/10.1051/0004-6361/201117055)
- Pinsonneault, M. H., Elsworth, Y. P., Tayar, J., et al. 2018, *ApJS*, 239, 32, doi: [10.3847/1538-4365/aabebfd](https://doi.org/10.3847/1538-4365/aabebfd)

- Pope, B. J. S., White, T. R., Huber, D., et al. 2016, *MNRAS*, 455, L36, doi: [10.1093/mnras/slv143](https://doi.org/10.1093/mnras/slv143)
- Pope, B. J. S., Davies, G. R., Hawkins, K., et al. 2019, *ApJS*, 244, 18, doi: [10.3847/1538-4365/ab2c04](https://doi.org/10.3847/1538-4365/ab2c04)
- Queiroz, A. B. A., Anders, F., Santiago, B. X., et al. 2018, *MNRAS*, 476, 2556, doi: [10.1093/mnras/sty330](https://doi.org/10.1093/mnras/sty330)
- Refsdal, S., & Weigert, A. 1970, *A&A*, 6, 426
- Retterer, J. M., & King, I. R. 1982, *ApJ*, 254, 214, doi: [10.1086/159725](https://doi.org/10.1086/159725)
- Reyes, C., Stello, D., Hon, M., & Zinn, J. C. 2022, arXiv e-prints, arXiv:2202.05478. <https://arxiv.org/abs/2202.05478>
- Ricker, G. R., Winn, J. N., Vanderspek, R., et al. 2015, *Journal of Astronomical Telescopes, Instruments, and Systems*, 1, 014003, doi: [10.1117/1.JATIS.1.1.014003](https://doi.org/10.1117/1.JATIS.1.1.014003)
- Rodrigues, T. S., Bossini, D., Miglio, A., et al. 2017, *MNRAS*, 467, 1433, doi: [10.1093/mnras/stx120](https://doi.org/10.1093/mnras/stx120)
- Serenelli, A., Johnson, J., Huber, D., et al. 2017, *ApJS*, 233, 23, doi: [10.3847/1538-4365/aa97df](https://doi.org/10.3847/1538-4365/aa97df)
- Sharma, S., Stello, D., Bland-Hawthorn, J., Huber, D., & Bedding, T. R. 2016, *ApJ*, 822, 15, doi: [10.3847/0004-637X/822/1/15](https://doi.org/10.3847/0004-637X/822/1/15)
- Silva Aguirre, V., Bojsen-Hansen, M., Slumstrup, D., et al. 2018, *MNRAS*, 475, 5487, doi: [10.1093/mnras/sty150](https://doi.org/10.1093/mnras/sty150)
- Silva Aguirre, V., Stello, D., Stokholm, A., et al. 2020, *ApJL*, 889, L34, doi: [10.3847/2041-8213/ab6443](https://doi.org/10.3847/2041-8213/ab6443)
- Skumanich, A. 1972, *ApJ*, 171, 565, doi: [10.1086/151310](https://doi.org/10.1086/151310)
- Soubiran, C., Le Campion, J. F., Brouillet, N., & Chemin, L. 2020, *VizieR Online Data Catalog*, B/pastel
- Soubiran, C., Le Campion, J. F., Cayrel de Strobel, G., & Caillou, A. 2010, *A&A*, 515, A111, doi: [10.1051/0004-6361/201014247](https://doi.org/10.1051/0004-6361/201014247)
- Stassun, K. G., Oelkers, R. J., Pepper, J., et al. 2018, *AJ*, 156, 102, doi: [10.3847/1538-3881/aad050](https://doi.org/10.3847/1538-3881/aad050)
- Stassun, K. G., Oelkers, R. J., Paegert, M., et al. 2019, *AJ*, 158, 138, doi: [10.3847/1538-3881/ab3467](https://doi.org/10.3847/1538-3881/ab3467)
- Stello, D., Huber, D., Bedding, T. R., et al. 2013, *ApJL*, 765, L41, doi: [10.1088/2041-8205/765/2/L41](https://doi.org/10.1088/2041-8205/765/2/L41)
- Stello, D., Zinn, J., Elsworth, Y., et al. 2017, *ApJ*, 835, 83, doi: [10.3847/1538-4357/835/1/83](https://doi.org/10.3847/1538-4357/835/1/83)
- Stello, D., Saunders, N., Grunblatt, S., et al. 2021, arXiv e-prints, arXiv:2107.05831. <https://arxiv.org/abs/2107.05831>
- . 2022, *MNRAS*, 512, 1677, doi: [10.1093/mnras/stac414](https://doi.org/10.1093/mnras/stac414)
- Takeda, Y., & Tajitsu, A. 2014, *PASJ*, 66, 91, doi: [10.1093/pasj/psu066](https://doi.org/10.1093/pasj/psu066)
- Tayar, J., Claytor, Z. R., Huber, D., & van Saders, J. 2022, *ApJ*, 927, 31, doi: [10.3847/1538-4357/ac4bbc](https://doi.org/10.3847/1538-4357/ac4bbc)
- Themeßl, N., Kuzlewicz, J. S., García Saravia Ortiz de Montellano, A., & Hekker, S. 2020, in *Stars and their Variability Observed from Space*, ed. C. Neiner, W. W. Weiss, D. Baade, R. E. Griffin, C. C. Lovekin, & A. F. J. Moffat, 287–291
- Twicken, J. D., Jenkins, J. M., Seader, S. E., et al. 2016, *AJ*, 152, 158, doi: [10.3847/0004-6256/152/6/158](https://doi.org/10.3847/0004-6256/152/6/158)
- Ulrich, R. K. 1986, *ApJL*, 306, L37, doi: [10.1086/184700](https://doi.org/10.1086/184700)
- van Leeuwen, F. 2007, *A&A*, 474, 653, doi: [10.1051/0004-6361:20078357](https://doi.org/10.1051/0004-6361:20078357)
- von Braun, K., & Boyajian, T. 2017, *Extrasolar Planets and Their Host Stars* (Springer International Publishing), doi: [10.1007/978-3-319-61198-3](https://doi.org/10.1007/978-3-319-61198-3)
- Weiss, W. W., Moffat, A. F. J., Schwarzenberg-Czerny, A., et al. 2014, in *Precision Asteroseismology*, ed. J. A. Guzik, W. J. Chaplin, G. Handler, & A. Pigulski, Vol. 301, 67–68, doi: [10.1017/S1743921313014105](https://doi.org/10.1017/S1743921313014105)
- Wenger, M., Ochsenbein, F., Egret, D., et al. 2000, *A&AS*, 143, 9, doi: [10.1051/aas:2000332](https://doi.org/10.1051/aas:2000332)
- White, T. R., Silva Aguirre, V., Boyajian, T., et al. 2015, in *European Physical Journal Web of Conferences*, Vol. 101, European Physical Journal Web of Conferences, 06068, doi: [10.1051/epjconf/201510106068](https://doi.org/10.1051/epjconf/201510106068)
- White, T. R., Pope, B. J. S., Antoci, V., et al. 2017, *MNRAS*, 471, 2882, doi: [10.1093/mnras/stx1050](https://doi.org/10.1093/mnras/stx1050)
- White, T. R., Huber, D., Mann, A. W., et al. 2018, *MNRAS*, 477, 4403, doi: [10.1093/mnras/sty898](https://doi.org/10.1093/mnras/sty898)
- Winget, D. E., Hansen, C. J., Liebert, J., et al. 1987, *ApJL*, 315, L77, doi: [10.1086/184864](https://doi.org/10.1086/184864)
- Yu, J., Huber, D., Bedding, T. R., et al. 2018, *ApJS*, 236, 42, doi: [10.3847/1538-4365/aaaf74](https://doi.org/10.3847/1538-4365/aaaf74)
- Zinn, J. C. 2021, *AJ*, 161, 214, doi: [10.3847/1538-3881/abe936](https://doi.org/10.3847/1538-3881/abe936)
- Zinn, J. C., Pinsonneault, M. H., Huber, D., et al. 2019, *ApJ*, 885, 166, doi: [10.3847/1538-4357/ab44a9](https://doi.org/10.3847/1538-4357/ab44a9)
- Zinn, J. C., Stello, D., Elsworth, Y., et al. 2020, *ApJS*, 251, 23, doi: [10.3847/1538-4365/abbee3](https://doi.org/10.3847/1538-4365/abbee3)
- . 2022, *ApJ*, 926, 191, doi: [10.3847/1538-4357/ac2c83](https://doi.org/10.3847/1538-4357/ac2c83)